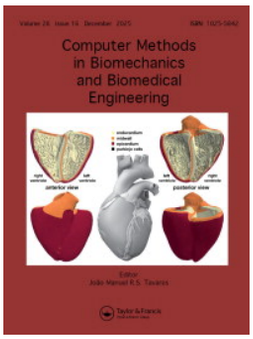

Taylor & Francis
Taylor & Francis Group

Computer Methods in Biomechanics and Biomedical Engineering

ISSN: 1025-5842 (Print) 1476-8259 (Online) Journal homepage: www.tandfonline.com/journals/gcmb20

The Lax–Friedrichs method in one-dimensional hemodynamics and its simplifying effect on boundary and coupling conditions

Anika Beckers & Niklas Kolbe

To cite this article: Anika Beckers & Niklas Kolbe (21 Jul 2025): The Lax–Friedrichs method in one-dimensional hemodynamics and its simplifying effect on boundary and coupling conditions, Computer Methods in Biomechanics and Biomedical Engineering, DOI: 10.1080/10255842.2025.2532027

To link to this article: https://doi.org/10.1080/10255842.2025.2532027

COMPUTER METHODS IN BIOMECHANICS AND BIOMEDICAL ENGINEERING
https://doi.org/10.1080/10255842.2025.2532027

The Lax–Friedrichs method in one-dimensional hemodynamics and its simplifying effect on boundary and coupling conditions

Anika Beckers and Niklas Kolbe

Institute of Geometry and Applied Mathematics, RWTH Aachen University, Aachen, Germany

ABSTRACT

The discretization of reduced one-dimensional hyperbolic models of blood flow using the Lax–Friedrichs method is discussed. Deriving the well-established scheme from a relaxation approach leads to new simplified boundary and coupling conditions in vascular networks accounting e.g. for vascular occlusions and bifurcations. In particular, blood flow modeling in networks of vessels can be realized with minimal information on the eigenstructure of the coupled models. The scheme, a MUSCL-type extension and the coupling conditions are obtained evaluating a discrete relaxation limit. Numerical experiments in uncoupled and coupled cases verify the consistency and convergence of the approach.

ARTICLE HISTORY
Received 30 January 2025
Accepted 2 July 2025

KEYWORDS
Blood flow modeling; cardiovascular networks; finite volumes; coupled conservation laws; boundary conditions; hyperbolic systems

2010 MSC
35L65; 35R02; 00A71; 62P10

1. Introduction

Over the last decades the number of cardiovascular disease cases in Europe has significantly increased; it nowadays accounts for 45 % of deaths in Europe (Wilkins et al. 2017). Among the concerned medical conditions stroke has been found to be responsible for most of the fatalities (Saini et al. 2021). Surgical treatments such as stent placements, coronary artery bypass grafting and endovascular thrombectomy relies on information about the patient specific hemodynamics, which accounts for the blood flow through the vasculature and the fluid-structure interaction with the vessel walls, see e.g. (Balossino et al. 2008; Forti et al. 2019).

Computational models have been shown to be useful tools for treatment development and operation planning, see (Crosetto et al. 2011; Neidlin et al. 2016) and the references therein. While accurate full-scale models in three space dimensions have been proposed, see e.g. (Hussain et al. 2025; Nobile and Vergara 2008), these models suffer from complexity and long run-times hampering clinical application. Reduced one-dimensional models based on simplifying assumptions on geometry and flow profiles, blood flow and interactions with the vessel wall have offered an efficient alternative (Formaggia et al. 2003; Hughes and Lubliner 1973). Those models, which are often stated in terms of hyperbolic systems of balance laws, have lately been increasingly used in applications ranging from uncertainty quantification in Fleeter et al. (2020) to simulating clinical interventions using intravascular catheters in Benemerito et al. (2023) and Pradhan et al. (2024).

Employing these models in real-time applications requires efficient numerical schemes. In the literature simulations have been carried out by Galerkin, e.g. (Mynard and Nithiarasu 2008; Steele et al. 2003), Taylor–Galerkin, cf. (Donea et al. 1984), or Godunov-type finite volume schemes, see e.g. (Formaggia et al. 2006; Müller and Toro 2013; Toro and Siviglia 2013; Wang et al. 2015). This work is concerned with the application of the Lax–Friedrichs method to cardiovascular models in one space dimension. The Lax–Friedrichs method introduced in Friedrichs and Lax (1971) belongs to the class of central schemes, cf. (Kurganov and Tadmor 2000)., and has been a popular

CONTACT Niklas Kolbe kolbe@igpm.rwth-aachen.de Institute of Geometry and Applied Mathematics, RWTH Aachen University, Templergraben 55, 52062 Aachen, Germany

Supplemental data for this article can be accessed online at https://doi.org/10.1080/10255842.2025.2532027.

choice for the solution of hyperbolic problems. Its main advantage is its universality, which is due to the fact that it is only loosely tied to the eigenstructure of the discretized problem (only an upper bound for the spectral radius of the system Jacobian is needed), and its conservative character. In the context of cardiovascular models this allows for a new simplified handling of domain boundaries and coupling conditions at vascular junctions in a network, which in Godunov-type schemes rely on the Lax-curves corresponding to the model. It facilitates the coupling, in particular, in model extensions accounting for blood solutes and endoscopic therapy for which Lax-curves might not be available. While this work introduces the general application and the correct handling of boundaries and network nodes, the companion paper (Herty et al. 2024) applies the approach to the modeling of aspiration therapy.

Typically, boundary conditions for the reduced one-dimensional models are based on the characteristic variables of the model and requires the extrapolation of the outgoing invariants and additional rules for the ingoing invariant (Formaggia et al. 2006; Peiró and Veneziani 2009). Conditions for the coupling of vessels at a junctions have been modeled in Formaggia et al. (2003). We also mention the recent approach from Lucca et al. (2023), in which the coupling has been modeled in more detail using a higher-dimensional sub-model. The coupling in our work and the derivation of the scheme will follow the approach from Herty et al. (2023), Herty et al. (2022) and employs the relaxation introduced in Jin and Xin (1995) for coupled hyperbolic systems. Discretizing the relaxed system using an implicit-explicit asymptotic preserving scheme recovers the Lax–Friedrichs scheme in the relaxation limit. Among others our approach allows us to couple the system for different velocity profiles encoded in different momentum-flux correction coefficients and to handle non-standard pressure models accounting for the viscoelasticity of the vessel wall.

The rest of the paper is structured as follows. In Section 2 we recall the reduced modeling of blood flow in a straight elastic vessel and thereby discuss two hyperbolic systems in different conserved variables. In Section 3 we consider the Xin-Jin-type relaxation of the blood flow models and use it to derive a Lax–Friedrichs type method. Also, a second-order extension using the MUSCL scheme is introduced, and an approximation is proposed that accounts for the diffusive term in the viscoelasticity considering model extension. In Section 4 we construct non-reflecting boundary data compatible with our approach. These do not require the extrapolation of the characteristic variables and can easily be extended to a higher order accuracy. Specific boundary conditions then result from imposing one of the key quantities, e.g. the pressure or the blood velocity, at the boundary. Section 5 progresses from the previously considered straight vessel to a vascular network by coupling various such vessels. A one-to-one coupling, which can deal with discontinuities in the vessel properties, and bifurcations in the vascular network are considered. The coupling conditions from Formaggia et al. (2003) are adjusted for an application within the presented scheme, similar to the handling of the boundary. Finally, in Section 6 numerical experiments are presented. Along with simulations of blood flow assuming entering pulse waves in the uncoupled and coupled case we verify our approach using grid convergence studies of our schemes with regard to the global spatial error and the coupling error at the interface.

2. Modeling of blood flow in an elastic vessel

In this section we discuss reduced one-dimensional models for blood flow in a single large vessel; vascular networks can be accounted for by coupling multiple vessels on decomposed domains, see e.g. (Formaggia et al. 2003). The considered vessel segment is assumed cylindrical, and the flow is described by an average axial velocity component. This allows for a model with state variables only depending on the time t and a single spatial variable x parameterizing the axis of the vessel. The model is obtained describing blood as a Newtonian fluid and averaging the compressible Navier–Stokes equations over the cross-sections of the elastic cylindrical domain, see e.g. (Hughes and Lubliner 1973) for details.

Denoting the cross-section area by $A = A(x,t)$ and the mass flux by $Q = Q(x,t)$, the model consists of the following two equations, accounting for mass conservation and momentum balance.

$$\begin{aligned} &\frac{\partial A}{\partial t} + \frac{\partial Q}{\partial x} = 0, \\ &\frac{\partial Q}{\partial t} + \frac{\partial}{\partial x}\left(\alpha \frac{Q^2}{A}\right) + \frac{A}{\rho}\frac{\partial p}{\partial x} = S_v(A,Q). \end{aligned} \tag{1}$$

In the second equation $p = p(x,t)$ denotes the space and time dependent pressure and ρ the constant blood density. The parameter α is the momentum-flux correction coefficient relating the averaged momentum to the actual momentum (Formaggia et al. 1999), and S_v is a source term accounting for the viscosity of blood. Both depend on the velocity profile within the cross-section; if we assume the profile to be independent of the axial position and radially symmetric, i.e. such that the

radial component of the velocity denoted by v depends only on the radial position r, we obtain

$$S_v(A,Q) = 2\mu R\left[\frac{\partial v}{\partial r}\right]_{r=R}, \qquad R = \sqrt{\frac{A}{\pi}} \tag{2}$$

with μ referring to the dynamic viscosity.

Commonly, Hagen–Poiseuille flow (White 1991) is assumed with the velocity profile

$$v = u\frac{\psi+2}{\psi}\left(1-\frac{r^\psi}{R^\psi}\right), \tag{3}$$

where u denotes the average axial velocity. Under this assumption the momentum-flux correction coefficient satisfies $\psi = (2-\alpha)/(\alpha-1)$. The choice $\psi = 9$ (and thus $\alpha = 1.1$) has been found to fit well to experimental data in Smith et al. (2002).

2.1. Vascular pressure

The pressure exerted on the vessel is dominated by forces due to the vessel wall displacement (Peiró and Veneziani 2009). This is reflected in the algebraic pressure law

$$p = P_{\text{ext}} + \beta\left(\sqrt{A}-\sqrt{A_0}\right), \tag{4}$$

where P_{ext} is a constant external pressure and $\beta = \frac{\sqrt{\pi}h_0E}{(1-\nu^2)A_0}$ with A_0 denoting the reference section area and h_0 the wall thickness, respectively. Moreover, ν is the Poisson ratio and E is the Young modulus corresponding to the vessel. A typical choice for the Poisson ratio is $\nu = 0.5$, reflecting the incompressibility of the wall tissue (Formaggia et al. 2003). The pressure law (4) assumes that the wall reacts immediately to compressive forces at the appropriate location. Additionally taking into account the viscoelasticity of the vessel wall by adopting a Voigt–Kelvin model (Fung and Cowin 1994) gives rise to the pressure

$$\tilde{p} = P_{\text{ext}} + \beta\left(\sqrt{A}-\sqrt{A_0}\right) + \frac{\gamma\sqrt{\pi}}{2\sqrt{A_0}^3}\frac{\partial A}{\partial t} \tag{5}$$

with γ being the viscoelasticity coefficient. Assuming that A_0 and γ are constant we can employ the first equation in (1) to rewrite the last term in (5) and obtain a parabolic model, in which the term

$$\frac{\gamma\sqrt{\pi}A}{2\rho\sqrt{A_0}^3}\frac{\partial^2 Q}{\partial x^2} \tag{6}$$

is added to the right-hand side of the second equation in (1).

2.2. Velocity form

As it holds $Q = Au$ for the mass flow basic algebra can be used to replace the *flow form* (1) by rewriting the model in the *velocity form*

$$\begin{aligned}&\frac{\partial A}{\partial t}+\frac{\partial Au}{\partial x} = 0,\\ &\frac{\partial u}{\partial t}+(2\alpha-1)u\frac{\partial u}{\partial x}+(\alpha-1)\frac{u^2}{A}\frac{\partial A}{\partial x}+\frac{1}{\rho}\frac{\partial p}{\partial x} = \frac{1}{A}S_v(A,Au).\end{aligned} \tag{7}$$

This model formulation has been particularly useful for the design of coupling conditions on a network, see e.g. Formaggia et al. (2003). While in the following we will base our study on the flow form (1) implications for the velocity form (7) will be discussed as well.

2.3. Conservative form

Being derived from basic principles, model (1) admits a conservative form[1]. This is made clear, using the antiderivative of the pressure function (4), i.e.

$$P(A) = A_0P_{\text{ext}} + \int_{A_0}^{A} p(a)da,$$

and writing the second equation in (1) as

$$\frac{\partial Q}{\partial t}+\frac{\partial}{\partial x}\left(\alpha\frac{Q^2}{A}+\frac{1}{\rho}(Ap-P)\right) = S_v(A,Q). \tag{8}$$

The velocity form (7) on the other hand does not always admit a conservative form, as the following proposition shows.

Proposition 2.1. *System (7) is conservative if and only if* $\alpha = 1$.

Proof. If $\alpha = 1$ we can write the second equation in (7) as

$$\frac{\partial u}{\partial t}+\frac{\partial}{\partial x}\left(\frac{1}{2}u^2+\frac{p}{\rho}\right) = \frac{1}{A}S_v(A,Au)$$

and thus (7) is conservative. Next, let $\alpha \neq 1$. We can generally rewrite the second equation in (7) as

$$\begin{aligned}&\frac{\partial u}{\partial t}+(2\alpha-1)u\frac{\partial u}{\partial x}+\left((\alpha-1)\frac{u^2}{A}+\frac{1}{\rho}\frac{\partial p}{\partial A}\right)\frac{\partial A}{\partial x}\\ &\quad = \frac{1}{A}S_v(A,Au).\end{aligned} \tag{9}$$

We assume in (9) that neither β nor A_0 vary in space. Next, we suppose that the system was conservative. Then there would be a smooth function f in the variables A and u such that

$$\frac{\partial u}{\partial t}+\frac{\partial f(A,u)}{\partial x} = \frac{1}{A}S_v(A,Au).$$

Due to (9) it would hold

$$T^A(A,u) := (\alpha-1)\frac{u^2}{A} + \frac{1}{\rho}\frac{\partial p}{\partial A} = \frac{\partial f(A,u)}{\partial A},$$
$$T^u(A,u) := (2\alpha-1)u = \frac{\partial f(A,u)}{\partial u}.$$

But since

$$\frac{\partial^2 f(A,u)}{\partial A \partial u} = \frac{\partial^2 f(A,u)}{\partial u \partial A}$$

and

$$\frac{\partial T^A(A,u)}{\partial u} = 2(\alpha-1)\frac{u}{A} \neq 0 = \frac{\partial T^u(A,u)}{\partial A}$$

we would arrive at a contradiction. Thus the system cannot be conservative. □

Remark 2.2. *If $\alpha = 1$ then system (7) would also be conservative for more general pressure functions, e.g. in the case that p depends also on u. Note that in this case (1) might not be conservative.*

In this work we assume that the reference section area as well as the wall parameter β are constant. We note though that smooth spatial variation in these parameters can be accounted for using additional source terms in the second equation *in (1) or (7), respectively*, which do not affect the conservation properties.

3. The Lax–Friedrichs method as a relaxation limit

In this section we consider a relaxation of the blood flow model from Section 2 along with a discretization that recovers the Lax–Friedrichs scheme in the relaxation limit.

3.1. The relaxation system

For the sake of brevity, the following analysis relies on the vector notation

$$\mathbf{U} = (A,Q)^T, \quad \mathbf{F}(\mathbf{U}) = \left(Q, \alpha\frac{Q^2}{A} + \frac{1}{\rho}(Ap - P)\right)^T,$$
$$\mathbf{S}(\mathbf{U}) = (0, S_v(A,Q))^T, \tag{10}$$

which allows us to express model (1) as the 2×2 system of balance laws

$$\frac{\partial \mathbf{U}}{\partial t} + \frac{\partial \mathbf{F}(\mathbf{U})}{\partial x} = \mathbf{S}(\mathbf{U}). \tag{11}$$

Introducing now the new variable $\mathbf{V} = (V^A, V^Q)^T$ mapping the time and space variables to $\mathbb{R}^2$ we follow Jin and Xin (1995) to obtain for any $\varepsilon > 0$ the Jin–Xin-type relaxation system

$$\begin{aligned} \frac{\partial \mathbf{U}}{\partial t} + \frac{\partial \mathbf{V}}{\partial x} &= \mathbf{S}(\mathbf{U}), \\ \frac{\partial \mathbf{V}}{\partial t} + \lambda^2 \frac{\partial \mathbf{U}}{\partial x} &= \frac{1}{\varepsilon}(\mathbf{F}(\mathbf{U}) - \mathbf{V}). \end{aligned} \tag{12}$$

If the relaxation speed λ is chosen as an upper bound of the system Jacobian, in particular

$$\lambda \geq \alpha\frac{Q}{A} \pm \sqrt{\alpha(\alpha-1)\frac{Q^2}{A^2} + \frac{\beta}{2\rho}\sqrt{A}}, \tag{13}$$

the subcharacteristic condition verifying the stability of (12) holds, see Liu (1987) for details. In the asymptotic relaxation limit $\varepsilon \to 0$ the auxiliary variable $\mathbf{V}$ approaches $\mathbf{F}(\mathbf{U})$ and $\mathbf{U}$ solves the original problem (11), see Chen et al. (1994). Numerical schemes for (12) that preserve this limit property have been of high interest (Hu et al. 2017). The unsplit scheme proposed in Jin (2012) is such a scheme, which we consider in more detail.

3.2. Discretization of the relaxation system

Let a uniform partition of the real line into the mesh cells $I_j = (x_{j-1/2}, x_{j+1/2})$ of width Δx be given. Additionally, we consider the time instances $t^n = \sum_{i=1}^n \Delta t^i$ and the time step sizes Δt^i. We approximate the vector valued states of (12) by volume averages over the cell I_j at time t^n that we denote as $\mathbf{U}_j^n$ and $\mathbf{V}_j^n$ and adopt an analogue notation for its components. The time step sizes are computed using the condition

$$\Delta t^n = \mathrm{CFL}\frac{\Delta x}{\lambda^n}, \tag{14}$$

where $\lambda^n = \max_j |\lambda_j^n|$ with λ_j^n denoting the right hand side of (13) evaluated with respect to the numerical solution in cell I_j at time t^n and given a suitable Courant number $0 < \mathrm{CFL} \leq 1$. For brevity we neglect the time index of the time step size and the relaxation speed in the following. Then the scheme reads

$$\begin{aligned} \mathbf{U}_j^{n+1} &= \mathbf{U}_j^n - \frac{\Delta t}{2\Delta x}\left(\mathbf{V}_{j+1}^n - \mathbf{V}_{j-1}^n\right) \\ &\quad + \frac{\lambda \Delta t}{2\Delta x}\left(\mathbf{U}_{j+1}^n - 2\mathbf{U}_j^n + \mathbf{U}_{j-1}^n\right) + \Delta t S(\mathbf{U}_j^n), \\ \mathbf{V}_j^{n+1} &= \mathbf{V}_j^n - \frac{\lambda^2 \Delta t}{2\Delta x}\left(\mathbf{U}_{j+1}^n - \mathbf{U}_{j-1}^n\right) \\ &\quad + \frac{\lambda \Delta t}{2\Delta x}\left(\mathbf{V}_{j+1}^n - 2\mathbf{V}_j^n + \mathbf{V}_{j-1}^n\right) \\ &\quad + \frac{\Delta t}{\varepsilon}\left(\mathbf{F}(\mathbf{U}_j^{n+1}) - \mathbf{V}_j^{n+1}\right). \end{aligned} \tag{15}$$

We note that the scheme has been derived from an upwind discretization of (12) in characteristic variables and an implicit-explicit time discretization. The implicit time discretization in the second equation of (15) is necessary to obtain an asymptotic preserving scheme, cf. (Hu et al. 2017), but does not require the solution of a nonlinear system as $\mathbf{U}_j^{n+1}$ can be computed independently. See Herty et al. (2023), Hu et al. (2017), and Jin and Xin (1995) for further details on the derivation of this scheme.

3.2.1. The limit scheme

As we take the limit $\varepsilon \to 0$ in (15) we obtain the scheme

$$\mathbf{U}_j^{n+1} = \mathbf{U}_j^n - \frac{\Delta t}{\Delta x}\left(\mathcal{F}_{j+1/2}^n - \mathcal{F}_{j-1/2}^n\right) + \Delta t S(\mathbf{U}_j^n) \quad (16)$$

for the original problem (11) with numerical fluxes given by

$$\mathcal{F}_{j-1/2}^n = \frac{1}{2}\left(\mathbf{V}_{j-1}^n + \mathbf{V}_j^n\right) - \frac{\lambda}{2}\left(\mathbf{U}_j^n - \mathbf{U}_{j-1}^n\right), \qquad \mathbf{V}_j^n = \mathbf{F}(\mathbf{U}_j^n) \quad \forall j \in \mathbb{Z}. \quad (17)$$

Refer to Herty et al. (2023) for the detailed limit procedure. Taking into account (14) the classical Lax–Friedrichs method is recovered taking CFL = 1.

3.2.2. High resolution extension

To increase the accuracy in space we use the MUSCL scheme (van Leer 1979) that employs slope reconstructions. Here we apply the approach to the characteristic variables of the relaxation system (12) implying that four scalar quantities are linearly reconstructed. This discretization gives rise to the high order correction terms

$$\mathcal{H}_{j-1/2}^{\text{MUSCL}} = \frac{\Delta x}{2}\left(\mathbf{s}_{j-1}^{n,-} - \mathbf{s}_j^{n,+}\right) \quad \forall j \in \mathbb{Z} \quad (18)$$

to be added to the numerical fluxes (17). We use the minmod limiter to prevent oscillatory behavior of the scheme. The reconstructed slopes in (18) thus take the form

$$\mathbf{s}_j^{n,\pm} := \operatorname{minmod}\left(\frac{\mathbf{V}_j^n - \mathbf{V}_{j-1}^n \pm \lambda(\mathbf{U}_j^n - \mathbf{U}_{j-1}^n)}{2\Delta x}, \frac{\mathbf{V}_{j+1}^n - \mathbf{V}_j^n \pm \lambda(\mathbf{U}_{j+1}^n - \mathbf{U}_j^n)}{2\Delta x}\right), \quad (19)$$

where the *minmod* operator is given by

$$\operatorname{minmod}(a,b) = \begin{cases} 0 & \text{if } \operatorname{sign}(a) \neq \operatorname{sign}(b) \\ a & \text{if } |a| \leq |b| \text{ and } \operatorname{sign}(a) = \operatorname{sign}(b) \\ b & \text{if } |a| > |b| \text{ and } \operatorname{sign}(a) = \operatorname{sign}(b) \end{cases}$$

for scalar arguments $a, b \in \mathbb{R}$ and component-wise in case of vectors.

3.3. Implications for the velocity form and extended pressure models

In this section we sketch how our relaxation based scheme derivation can be applied to model (7) and how the extended pressure law (5) is treated numerically.

3.3.1. Velocity form

The above approach is also applicable to the blood flow model in velocity form (7) in the case $\alpha = 1$ by taking

$$\mathbf{U} = (A,u)^T, \qquad \mathbf{F}(\mathbf{U}) = \left(Au, \frac{1}{2}u^2 + \frac{p}{\rho}\right)^T, \qquad \mathbf{S}(\mathbf{U}) = \left(0, \frac{1}{A}S_v(A,Q)\right)^T \quad (20)$$

instead of (10) in (11). To satisfy the subcharacteristic condition in this case, it is sufficient to choose the relaxation speed λ such that (13) holds for $\alpha = 1$. If $\alpha \neq 1$ the generalized relaxation approach from Kolbe et al. (2024) relying on path-conservative schemes can be applied to system (7).

3.3.2. Viscoelasticity

In the case that viscoelasticity is considered within model (1) by means of the extended pressure law (5) the additional second order term (6) is approximated by the semi-implicit finite difference formula

$$R_j(\mathbf{U}^n, \mathbf{U}^{n+1}) = \frac{\gamma\sqrt{\pi}A_j^n}{2\rho\sqrt{A_0}^3}\,\frac{Q_{j+1}^{n+1} - 2Q_j^{n+1} + Q_{j-1}^{n+1}}{\Delta x^2}. \quad (21)$$

To simulate the augmented model we add $(0, \Delta t R_j(\mathbf{U}^n, \mathbf{U}^{n+1}))^T$ to the right-hand side of scheme (16), which results in a linear system that is to be solved in each time step. As the system matrix is tridiagonal we use the Thomas algorithm to efficiently solve the system within our scheme. Note that we can also apply the high order extension (18) to this case of using the extended pressure law (5).

4. Boundary conditions

In this section we discuss appropriate boundary conditions for scheme (16). Boundary conditions for the blood flow model (1) can account for different scenarios, see e.g. (Formaggia et al. 2006). Among others, they may account for inflow at the proximal boundary due to a heartbeat, see e.g. the approach in Formaggia et al. (2006) distinguishing between the

diastolic and the systolic phase. At the distal boundary an outflow can be modeled incorporating reflections in the entire vascular periphery. These reflections bring forth smaller waves traveling against the main direction of blood flow. This can be taken into account using single-resistance or three-element *Windkessel* models (Peiró and Veneziani 2009). The boundary conditions may also describe an occlusion of the vessel. The new boundary conditions we construct here need to account for the fact that the employed Lax–Friedrichs scheme is derived from relaxation system (12) and thus constitute suitable boundary data for this system (Dubois and Le Floch 1988). In particular, this means that not only boundary states with respect to the original state $\mathbf{U}$ but also with respect to the variable $\mathbf{V}$ are required. If the extended pressure model (5) is used, we assume that the problem remains convection dominated and neglect the parabolic term at the boundaries and vessel interconnections, both numerically and in the construction of boundary and coupling states for the convective part of the model.

In the following we consider blood flow on the bounded domain (a, b) discretized by scheme (16) over N mesh cells $I_1, \dots, I_N$ such that a is located at the left boundary of I_1 and b at the right boundary of I_N. Given the cell averages $\mathbf{U}_1^n, \dots, \mathbf{U}_N^n$ and fluxes $\mathbf{V}_1^n, \dots, \mathbf{V}_N^n$ the boundary states $\mathbf{U}_L^n$, $\mathbf{V}_L^n$, $\mathbf{U}_R^n$, $\mathbf{V}_R^n$ for the computation of $\mathcal{F}_{1/2}^n$ and $\mathcal{F}_{N+1/2}^n$ according to (17) are sought in order to update the numerical solution to the time instance t^{n+1}. These states serve as Dirichlet boundary data for the solution update from instance t^n to t^{n+1}, or equivalently as (piecewise constant) ghost cells beyond the boundaries. For brevity, we drop the time index in the following discussion. The situation is visualized in Figure 1. We make use of our findings from Herty et al. (2022) implying that suitable boundary data for the relaxation system satisfies the conditions

$$\mathbf{V}_L - \mathbf{V}_1 = \lambda(\mathbf{U}_L - \mathbf{U}_1) \qquad \text{and} \qquad \mathbf{V}_R - \mathbf{V}_N = \lambda(\mathbf{U}_N - \mathbf{U}_R). \tag{22}$$

Note that (22) resembles Rankine-Hugoniot conditions. Instead of using generalized Riemann invariants as in Godunov-type methods our approach relies on shock-relations and thus differs in its wave-structure assumption.

4.1. Non-reflecting boundary conditions

Typically, boundaries in the blood flow model are assumed to be non-reflecting, which implies that

$$\mathbf{l}_1(\mathbf{U}_L)^T \left.\frac{\partial \mathbf{F}(\mathbf{U})}{\partial x}\right|_{x=a} = 0 \qquad \text{and} \qquad \mathbf{l}_2(\mathbf{U}_R)^T \left.\frac{\partial \mathbf{F}(\mathbf{U})}{\partial x}\right|_{x=b} = 0 \tag{23}$$

holds, where $\mathbf{l}_1$ and $\mathbf{l}_2$ denote the left eigenvectors corresponding to the negative and positive eigenvalue of the system (11), respectively, see Thompson (1987). This has been addressed in the literature *via* extrapolation of the outgoing Riemann invariant within Taylor–Galerkin schemes, see Quarteroni and Formaggia (2004); we consider an alternative approach more suitable for our numerical method. In the situation shown in Figure 1, where we have piecewise constant data, the derivatives in (23) can be approximated by a central difference with respect to a small increment $\delta < \Delta x$ so that after eliminating the denominator we obtain

$$\mathbf{l}_1(\mathbf{U}_L)^T[\mathbf{F}(\mathbf{U}_1) - \mathbf{F}(\mathbf{U}_L)] = 0 \text{ and } \mathbf{l}_2(\mathbf{U}_R)^T[\mathbf{F}(\mathbf{U}_R) - \mathbf{F}(\mathbf{U}_N)] = 0. \tag{24}$$

Next, employing (24) to formulate a consistent condition in the variable $\mathbf{V}$, cf. (Herty et al. 2023), and using (22) we derive the conditions

$$\begin{aligned} Q_1 - Q_L &= \left(\alpha\frac{Q_L}{A_L} + \sqrt{\alpha(\alpha-1)\frac{Q_L^2}{A_L^2} + \frac{\beta}{2\rho A_0}\sqrt{A_L}}\right)(A_1 - A_L), \\ Q_N - Q_R &= \left(\alpha\frac{Q_R}{A_R} - \sqrt{\alpha(\alpha-1)\frac{Q_R^2}{A_R^2} + \frac{\beta}{2\rho A_0}\sqrt{A_R}}\right)(A_N - A_R) \end{aligned} \tag{25}$$

for system (1), and under the assumption $\alpha = 1$ the conditions

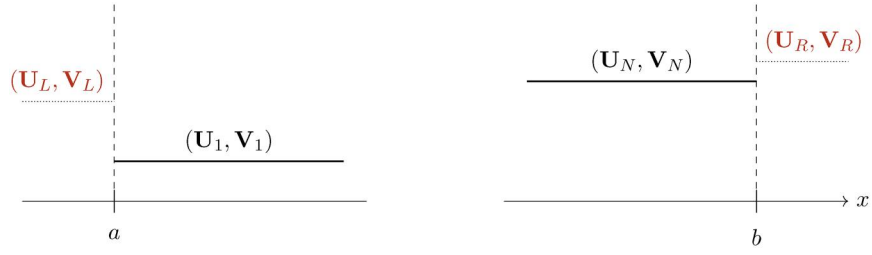

Figure 1. The relaxation system at the boundaries. The states $\mathbf{U}_L$, $\mathbf{V}_L$, $\mathbf{U}_R$ and $\mathbf{V}_R$ constitute suitable boundary data with respect to the cell averages $\mathbf{U}_1$, $\mathbf{V}_1$, $\mathbf{U}_N$, $\mathbf{V}_N$ of the numerical solution.

Figure 2. One-to-one (left) and one-to-two (right) vascular junction.

$$u_1 - u_L = A_L^{-3/4}\sqrt{\frac{\beta}{2\rho}}(A_1 - A_L),$$

$$u_N - u_R = -A_L^{-3/4}\sqrt{\frac{\beta}{2\rho}}(A_N - A_R) \tag{26}$$

for system (7).

4.2. Prescribed pressure, mass flow and velocity at the boundary

For well-posedness at the boundary additional conditions complementing (25) or (26) are needed. In some application a boundary pressure p_L or p_R is imposed. In this case the boundary section area can be deduced inverting the pressure law (4), i.e. taking $A_L = p^{-1}(p_L)$ or $A_R = p^{-1}(p_R)$. The corresponding mass flow / velocity is then computed from (25)/(26) solving a linear equation if $\alpha = 1$ or a quadratic one after eliminating the square root if $\alpha \neq 1$.

In other applications a boundary velocity u_L or u_R might be imposed. If the model is given in velocity form and $\alpha = 1$ then the corresponding section area at the boundary can be computed from (26), which after eliminating all fractional exponents involves the solution of a quartic equation. If the model is given in flow form we first rewrite $Q = Au$ in (26) and afterwards similarly solve the corresponding equation for A_L or A_R. In the special case of a reflecting boundary, i.e. $u_L = 0$ or $u_R = 0$, this computation significantly simplifies.

The above techniques are used for instance to model a beating heart. Therefore, one alternates in time between imposing a sinusoidal inlet pressure while the valve is open, see e.g. below, and reflecting boundary conditions at the inlet when the valve is closed (Formaggia et al. 2006). Alternatively the vessel can be coupled to a time-varying elastance model for the left ventricle, see e.g. (Segers et al. 2003). These procedures have always led to a single real solution for the boundary value in all our numerical computations employing relevant parameters. After the boundary state $\mathbf{U}_L$ or $\mathbf{U}_R$ has been determined the corresponding boundary state in the variable $\mathbf{V}$ is derived from (22).

5. Coupling in a vascular network

A full arterial network with bifurcations, curvatures and discontinuities in wall properties may be approximated by a graph with edges representing straight vessel segments. In addition, suitable boundary conditions at the nodes are required that connect the flow dynamics of the incoming and outgoing edges. In the following we discuss some of these *coupling conditions* in the basic cases shown in Figure 2 and embed them in the relaxation form (12) that is used within our scheme. We thereby focus on model (1) and without loss of generality assume $P_{\text{ext}} = 0$.

5.1. One-to-one coupling

To model discontinuities in vessel properties as they might occur e.g. in the presence of a stent, the domain is typically decomposed and two segments with different model parameters are coupled at an interface, as visualized in Figure 2 (left). In this situation conditions are required to determine the boundary states $\mathbf{U}_R^n$ and $\mathbf{V}_R^n$ for the left coupled vessel as well as $\mathbf{U}_L^n$ and $\mathbf{V}_L^n$ for the right coupled vessel at the interface. These states are used for the update of the numerical solution at the interface. As in Section 4 we neglect the time index in the following.

Based on Formaggia et al. (2003) we impose continuity of both, mass flux and generalized total pressure[2] defined by $p_t = \alpha\frac{\rho}{2}(\frac{Q}{A})^2 + p$, i.e. the coupling conditions

$$Q_R = Q_L, \tag{27}$$

$$\alpha\ \frac{\rho}{2}\left(\frac{Q_R}{A_R}\right)^2 + p\left(A_R; A_0^I, \beta^I\right) = \alpha\ \frac{\rho}{2}\left(\frac{Q_L}{A_L}\right)^2 + p\left(A_L; A_0^{II}, \beta^{II}\right) \tag{28}$$

hold. Here, the reference section area and the wall parameter in the pressure law may depend on the vessel and we employ the notations A_0^I and β^I to refer to the parameters of the incoming vessel on the left and A_0^{II} and β^{II} to refer to the parameters of the outgoing vessel on the right, respectively. We note that in addition to the conditions that we consider here, extended conditions are available that take into account the coupling angle, see Formaggia et al. (2003).

5.1.1. Coupling the relaxation system

In our relaxation approach coupling conditions for the auxiliary variables $\mathbf{V}$ are additionally required to provide all boundary values in scheme (16). To numerically approximate the networked system using this scheme we alternate between computing the boundary/coupling data and updating the numerical solution on all edges. We employ the consistency principle introduced in Herty et al. (2023) to derive suitable conditions.

As the variable V^A represents the first component of the flux $\mathbf{F}(\mathbf{U})$, condition (27) implies the consistent condition

$$V_R^A = V_L^A. \tag{29}$$

Similarly, a condition for the variable V^Q is derived using (28). Taking into account the flux in (8) we obtain

$$\begin{aligned} &A_R^{-1}\left[V_R^Q - \frac{\alpha}{2}\frac{Q_R^2}{A_R} + \rho^{-1}\ P(A_R; A_0^I, \beta^I)\right] \\ &\quad = A_L^{-1}\left[V_L^Q - \frac{\alpha}{2}\frac{Q_L^2}{A_L} + \rho^{-1}\ P(A_L; A_0^{II}, \beta^{II})\right]. \end{aligned} \tag{30}$$

To eventually obtain the coupling data, a solution of the nonlinear system given by (27–30) and (22) needs to be computed. To this end we first eliminate the variables within $\mathbf{V}_R$ and $\mathbf{V}_L$ using (22) in (29) and (30) and then solve the remaining system for the variables within $\mathbf{U}_R$ and $\mathbf{U}_L$. We provide a detailed algorithm for the solution of the system in Appendix A.

Remark 5.1. *Assuming zero-flux conditions at the left boundary of vessel I and at the right boundary of vessel II the total mass with respect to the section area A is preserved by our scheme. A simple computation shows that for the first component of the right outgoing flux in vessel I and the left incoming flux in vessel II it holds*

$$\left[\mathcal{F}^I_{N+1/2}\right]_1 = V_R^A \quad \text{and} \quad \left[\mathcal{F}^I_{1+1/2}I\right]_1 = V_L^A.$$

The discrete conservation of mass then follows from (29).

5.1.2. Velocity formulation

In analogy to the above derivation, coupling conditions for the *velocity form* and $\alpha = 1$ are derived, which read

$$\begin{aligned} A_R u_R &= A_L u_L, \\ \frac{\rho}{2}u_R^2 + p\left(A_R; A_0^I, \beta^I\right) &= \frac{\rho}{2}u_L^2 + p\left(A_L; A_0^{II}, \beta^{II}\right), \\ V_R^A &= V_L^A, \\ V_R^u &= V_L^u. \end{aligned}$$

Again, solving this system taking (22) into account gives rise to the boundary fluxes within scheme (16) for the coupled system (7).

5.2. One-to-two coupling

This section is concerned with bifurcations i.e. vascular junctions, at which one vessel is divided into two as shown in Figure 2 (right). In the following, we indicate for all quantities the corresponding vessel of the junction using an index from I to III as marked in the figure. Boundary/coupling data are sought at the right boundary for vessel I and at the left boundaries for vessels II and III. Following Formaggia et al. (2003) we impose conservation of mass flow and continuity of total pressure at the coupling node:

$$Q_R^I = Q_L^{II} + Q_L^{III}, \tag{31}$$

$$\alpha\ \frac{\rho}{2}\left(\frac{Q_R^I}{A_R^I}\right)^2 + p\left(A_R^I; A_0^I, \beta^I\right) = \alpha\ \frac{\rho}{2}\left(\frac{Q_L^{II}}{A_L^{II}}\right)^2 + p\left(A_L^{II}; A_0^{II}, \beta^{II}\right), \tag{32}$$

$$\alpha\ \frac{\rho}{2}\left(\frac{Q_R^I}{A_R^I}\right)^2 + p\left(A_R^I; A_0^I, \beta^I\right) = \alpha\ \frac{\rho}{2}\left(\frac{Q_L^{III}}{A_L^{III}}\right)^2 + p\left(A_L^{III}; A_0^{II}, \beta^{II}\right). \tag{33}$$

In addition, we propose new conditions for the variable $\mathbf{V}$ to be used within scheme (16). Relying again on the consistency principle in the relaxation limit gives rise to

$$V_R^{A,I} = V_L^{A,II} + V_L^{A,III} \tag{34}$$

when considering the original condition (31). In analogy to (30) we further derive conditions for the variable V^Q that read

$$\begin{aligned} &\frac{A_L^{II}}{A_R^I}\left[V_R^{Q,I} - \frac{\alpha}{2}\frac{(Q_R^I)^2}{A_R^I} + \rho^{-1}\ P(A_R^I; A_0^I, \beta^I)\right] \\ &\quad = V_L^{Q,II} - \frac{\alpha}{2}\frac{(Q_L^{II})^2}{A_L^{II}} + \rho^{-1}\ P(A_L^{II}; A_0^{II}, \beta^{II}), \end{aligned} \tag{35}$$

$$\begin{aligned} &\frac{A_L^{III}}{A_R^I}\left[V_R^{Q,I} - \frac{\alpha}{2}\frac{(Q_R^I)^2}{A_R^I} + \rho^{-1}\ P(A_R^I; A_0^I, \beta^I)\right] \\ &\quad = V_L^{Q,III} - \frac{\alpha}{2}\frac{(Q_L^{III})^2}{A_L^{III}} + \rho^{-1}\ P(A_L^{III}; A_0^{III}, \beta^{III}). \end{aligned} \tag{36}$$

To compute the coupling data in practice, the full system is solved for the coupling states $\mathbf{U}_R^I$, $\mathbf{U}_L^{II}$ and $\mathbf{U}_L^{III}$ after component-wise substituting

$$\begin{aligned} \mathbf{V}_R^I &= \mathbf{V}_N^I + \lambda(\mathbf{U}_N^I - \mathbf{U}_R^I), \\ \mathbf{V}_L^{II} &= \mathbf{V}_1^{II} + \lambda(\mathbf{U}_L^{II} - \mathbf{U}_1^{II}), \\ \mathbf{V}_L^{III} &= \mathbf{V}_1^{III} + \lambda(\mathbf{U}_L^{III} - \mathbf{U}_1^{III}) \end{aligned}$$

in (34, 36) and (36). We use the multidimensional Newton–Raphson method to solve this nonlinear system.

6. Numerical experiments

In this section we apply our numerical scheme (16) in combination with the derived boundary and coupling conditions in various numerical experiments to demonstrate the performance of our approach. Experiments on one (the uncoupled case) and two edges (one-to-one coupling) are considered and each edge is discretized over uniform mesh cells of size Δx. Fixed time steps are used that are given by (14), where the relaxation speed λ is chosen such that equality holds in (13). Each edge represents a 400 cm long vessel that is discretized over 800 grid points if not otherwise noted. Those unphysiologically long vessels have been chosen to better visualize the dynamics in the following. We fix CFL $= 1$ for the first order scheme resulting in the classical Lax–Friedrichs scheme; for our second order scheme CFL $= 0.2$ has lead to accurate results and robust computations. The code is implemented in the Julia programming language (Bezanson et al. 2017) on the basis of the implementation for the scheme (Kolbe 2022). The main parameters are chosen as $A_0 = 6.6$ cm^2, $h_0 = 0.26$ cm, $\nu = 0.5$, $\mu = 0$, $E = 2.43 \cdot 10^6$ dyne/cm^2, $\rho = 1.06$ g/cm^2, and $\alpha = 1$.

6.1. Single vessel tests

In this section we consider numerical experiments and tests of the uncoupled scheme, i.e. on a single edge.

6.1.1. Grid convergence

We study the convergence of our first and second order schemes from Section 3 in space. Therefore we use the method of manufactured solutions as proposed in Müller and Blanco (2015). In more details, we introduce the function

$$\begin{bmatrix} \hat{A}(x,t) \\ \hat{Q}(x,t) \end{bmatrix} = \begin{bmatrix} A^c + \delta A^c \sin\left(\frac{2\pi}{L}x\right)\cos\left(\frac{2\pi}{T}t\right) \\ Q^c - \delta A^c \frac{L}{T}\cos\left(\frac{2\pi}{L}x\right)\sin\left(\frac{2\pi}{T}t\right) \end{bmatrix} \tag{37}$$

that oscillate around the mean values A^c and Q^c with amplitude determined by the parameter δ. This function is a solution to the perturbed system

$$\frac{\partial \mathbf{U}}{\partial t} + \frac{\partial \mathbf{F}(\mathbf{U})}{\partial x} = \mathbf{S}(\mathbf{U}) + \overline{\mathbf{S}}(\mathbf{U}). \tag{38}$$

with appropriately chosen source term $\overline{\mathbf{S}}$, which we do not provide in detail here for brevity. Applying our scheme to this perturbed system we can compute the discretization error comparing with the exact solution. Within the second order MUSCL scheme (18) we have varied the Courant number with the time step taking CFL $= 0.49 \cdot \Delta x$ to avoid a reduction of the error due to the first order time discretization that we use and isolate the spatial error.

In our tests, we choose the parameters $Q^c = 10^{-4}$ m^3/s, $A^c = 14^2\pi$ mm^2, $\delta = 0.1$, $L = 1$ m and $T = 1$ s. We successively refine the grid and compute discrete L^1-errors in the quantities Q and A at time $t = 0.1$ with respect to the exact solution (37) and present them in Tables 1 and 2 for different test cases. Along we show the experimental order of convergence (EOC)[3].

First, we impose periodic boundary matching the periodicity of (37). The errors, reported in Table 1 clearly indicate linear and quadratic convergence of the first and second order scheme, respectively.

In a second test, we validate our coupling approach by coupling the numerical approximation to the exact solution. At the left boundary the left traces to be used to compute the coupling data following the steps in Section 5.1 is taken from the exact solution allowing us to compute the states $\mathbf{U}_L^n$ and $\mathbf{V}_L^n$ for the next update of the solution. At the right boundary we proceed analogously. The corresponding discretization errors are presented in Table 2. Linear convergence is again clearly indicated for the first order scheme. Due to the first order boundary treatment, second order convergence in this case is not expected. This is reflected in the results in Table 2. Nevertheless, comparing both schemes we observe a clear advantage of the second order scheme with respect to the errors.

Table 1. L^1 Errors at time $t = 0.1$ s for the flow rate Q in m^3/s and the section area a in m^2 under grid refinement with periodic boundary conditions.

		First order scheme		Second order scheme	
Quantity	num. cells	L^1-error	EOC	L^1-error	EOC
Q	32	3.87×10^{-5}		3.78×10^{-6}	
	64	1.96×10^{-5}	0.982	8.71×10^{-7}	2.118
	128	9.85×10^{-6}	0.99	2.15×10^{-7}	2.019
	256	4.94×10^{-6}	0.996	5.24×10^{-8}	2.037
	512	2.47×10^{-6}	0.998	1.31×10^{-8}	1.998
A	32	1.24×10^{-6}		3.58×10^{-7}	
	64	7.00×10^{-7}	0.821	$8.02\cdot10^{-8}$	2.157
	128	3.70×10^{-7}	0.919	$1.83\cdot10^{-8}$	2.133
	256	1.90×10^{-7}	0.961	$4.42\cdot10^{-9}$	2.048
	512	9.64×10^{-8}	0.981	$1.08\cdot10^{-9}$	2.037

6.1.2. Pulse propagation test

To further validate our scheme, we consider the single pulse propagation test proposed in Boileau et al. (2015). Here a Gaussian-shaped wave propagates through a single vessel, which is realized prescribing a temporal mass flow profile at the left vessel boundary. For the numerical approximation we employed the MUSCL scheme on uniform cells of 2.5 mm width using the Courant number CFL = 0.49. Figure 3 displays the position of the pulse wave at different time instances in experiments considering inviscid and viscous problems. In the latter case, the amplitude of the pulse decays following a theoretically determined exponential damping curve. These results are in good agreement with the numerical results obtained by a series of alternative schemes of different accuracy, see the comparison in Boileau et al. (2015).

Table 2. L^1 Errors at time $t = 0.1$ s for the flow rate Q in m^3/s and the section area a in m^2 under grid refinement employing a coupling to the exact solution at the boundaries.

		First order scheme		Second order scheme	
Quantity	Num. cells	L^1-error	EOC	L^1-error	EOC
Q	32	2.79×10^{-5}		4.29×10^{-6}	
	64	1.40×10^{-5}	0.99	1.10×10^{-6}	1.966
	128	7.03×10^{-6}	0.996	2.93×10^{-7}	1.905
	256	3.52×10^{-6}	0.998	9.37×10^{-8}	1.646
	512	1.763×10^{-7}	0.999	3.75×10^{-8}	1.319
A	32	1.81×10^{-6}		4.21×10^{-7}	
	64	1.00×10^{-6}	0.852	1.27×10^{-7}	1.73
	128	5.26×10^{-7}	0.927	3.90×10^{-8}	1.705
	256	2.70×10^{-7}	0.961	1.49×10^{-8}	1.387
	512	1.37×10^{-7}	0.981	6.72×10^{-9}	1.149

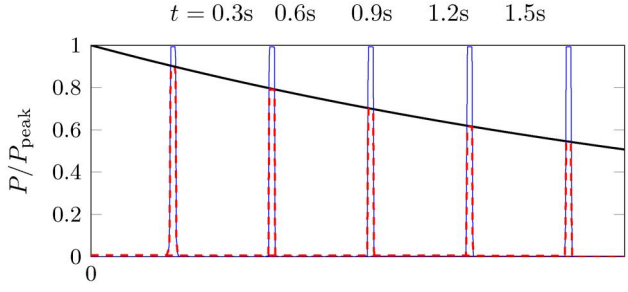

Figure 3. Normalized pressure in the single pulse propagation test showing its position at time instances 0.3s, 0.6s, 0.9s, 1.2s, 1.5s in an inviscid (blue solid lines) and a viscous (red dashed lines) problem. In the latter case, the amplitude of the pulse decays following a theoretically determined exponential damping curve (black solid line).

6.1.3. Viscoelasticity

Next, we investigate the impact of the extended pressure (6) taking into account the viscoelasticity of the vessel wall. To this end we revisit the previous experiment considering the entering pulse wave and compare numerical solutions of the classical model ($\gamma = 0$) and the extended pressure model (taking $\gamma = 120 \cdot \frac{A_0^{3/2}}{\sqrt{\pi}}$). In Figure 4 the numerical solution in terms of flow rate and section area at time instance $t = 0.4$ are shown. A significant smoothing effect of the viscoelasticity is exhibited in both, the flow rate and the section area, decreasing the amplitude of the pressure wave.

6.2. One-to-one coupling

In this section we consider two one-to-one coupling experiments studying discontinuities in different wall properties at the coupling node. In both experiments we use the initial data $A^I(\cdot,0) \equiv A_0^I$, $A^{II}(\cdot,0) \equiv A_0^{II}$ and $Q^I(\cdot,0) \equiv Q^{II}(\cdot,0) \equiv 0$, as boundary conditions we impose a pulse wave entering from the left boundary of vessel I and homogeneous Neumann conditions at the right boundary of vessel II. Both vessels are coupled at an interface as described in Section 5.1

Firstly, a discontinuity in the reference section area A_0 is assumed; in more details we assume $A_0^I = 1.25A_0$ on the left incoming vessel and $A_0^{II} = 0.75A_0$ on the right outgoing vessel. In Figure 5 we show mass flow, pressure, section area and velocity $u = Q/A$ at two different time steps. At time $t = 0.425$ we see some deflections at the coupling interface $x = 0$. Due to the reduced vessel diameter the blood is decelerated in front of the interface. Thus, the velocity and the mass flow are decreased, and the pressure and section area are increased at this position. This effect creates backward-propagating waves, which are visible at time $t = 0.6$ in addition to the first wave that has passed the interface.

The next experiment is concerned with a discontinuity in the vessel elasticity. In more details a transition from the stiffer vessel I to the more elastic vessel II is modeled by imposing the Young modulus $E^I =$

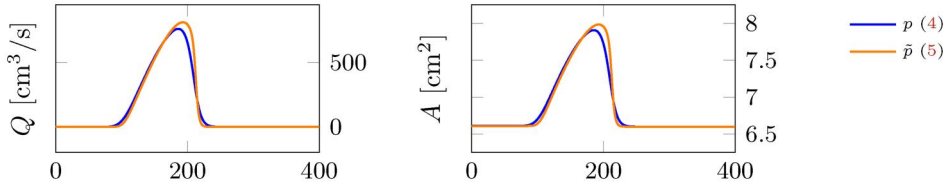

Figure 4. Flow rate Q and section area a over space (x-axis in cm) at time $t = 0.4$ using the classical pressure model (4) (orange) and the extended pressure model (5) (blue).

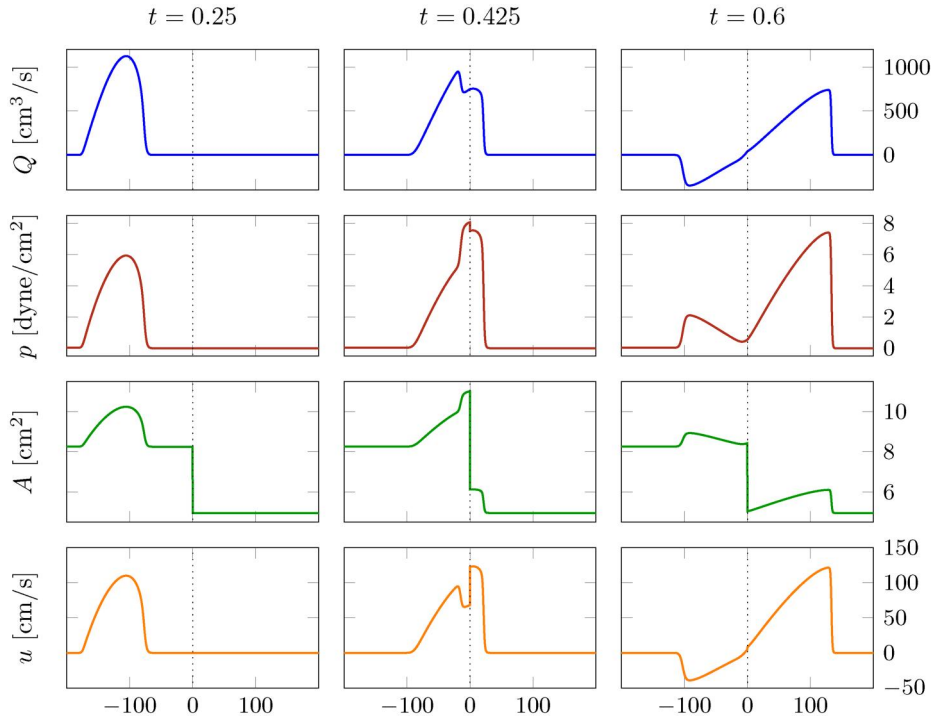

Figure 5. Flow rate Q, pressure p, section area a and velocity u over space (x-axis in cm) at time instances $t \in \{0.25, 0.425, 0.6\}$ over two vessels with different reference section areas ($A_0^I > A_0^{II}$) coupled at $x = 0$.

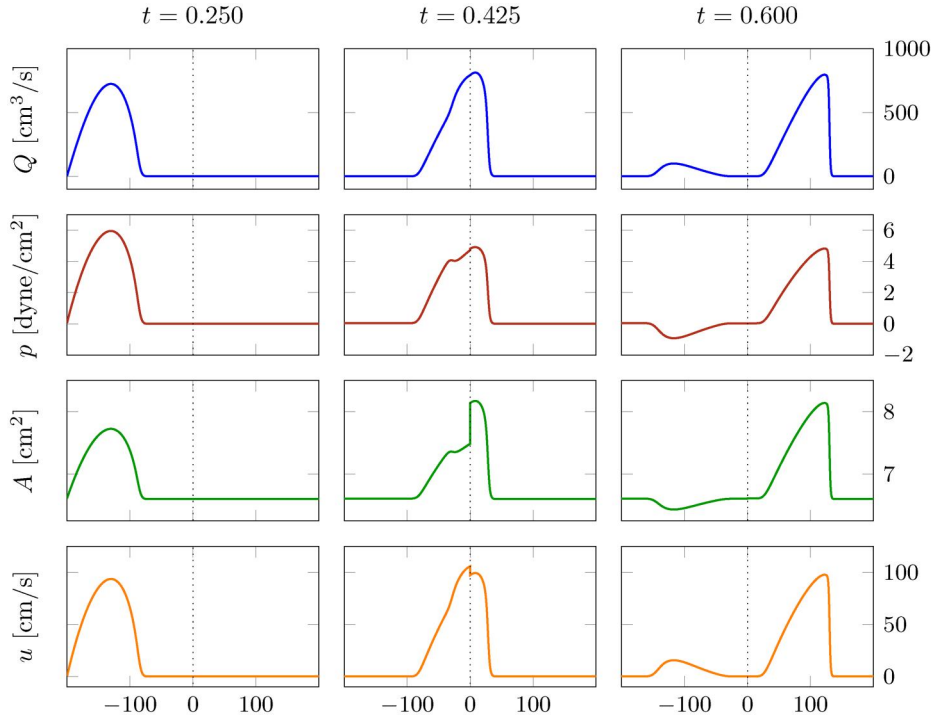

Figure 6. Flow rate Q, pressure p, section area a and velocity u over space (x-axis in cm) at time instances $t \in \{0.25, 0.425, 0.6\}$ over two vessels with different young modulus ($E^I < E^{II}$) coupled at $x = 0$.

$1.25E$ to the left and $E^{II} = 1.75E$ to the right vessel. In Figure 6 we show the numerical solution of this coupled experiment at two time instances. At time $t = 0.4$ the more elastic vessel is further extended as can be seen examining the section area near the interface. As a consequence the blood velocity in front of the discontinuity is increased, whereas the pressure is decreased there and the mass flux is increased. At time $t = 0.6$ the pressure wave has passed the interface and a backwards traveling wave appears from the

Table 3. Coupling errors defined in (39) under grid refinement in the experiments considering discontinuous A_0 and E.

	Discontinuous A_0				Discontinuous E			
N	e_1^c	EOC	e_2^c	EOC	e_1^c	EOC	e_2^c	EOC
50	48.265		2047.383		57.677		5155.836	
100	24.411	0.983	1006.360	1.025	21.565	1.419	1909.133	1.433
200	12.150	1.007	502.089	1.003	11.098	0.958	980.020	0.962
400	6.055	1.005	250.877	1.001	5.559	0.997	490.107	1.000
800	3.022	1.003	125.394	1.001	2.781	0.999	244.958	1.001
1600	1.509	1.002	62.685	1.000	1.391	1.000	122.462	1.000

interface causing a pressure decrease and a tightening of the vessel.

6.2.1. Coupling error

For consistency with the problem given by (1) on both vessels together with the coupling conditions (27) and (28) it is necessary that our numerical solution approximately satisfies the coupling condition. We test this by computing the errors

$$e_1^c = |Q_N^I - Q_1^{II}|,$$
$$e_2^c = \left|\alpha\ \frac{\rho}{2}\left(\frac{Q_N^I}{A_N^I}\right)^2 + p(A_N^I; A_0^I, \beta^I) - \alpha\ \frac{\rho}{2}\left(\frac{Q_1^{II}}{A_1^{II}}\right)^2 - p(A_1^{II}; A_0^{II}, \beta^{II})\right| \tag{39}$$

that quantify the approximation of the coupling conditions by substituting the numerical trace data next to the interface. In Table 3 those errors are shown for both test cases above under grid refinement at the fixed time instance $t = 0.5$, at which the pulse wave has reached the interface. In both experiments the EOCs indicate first order of convergence for both coupling errors confirming the consistency of our approach.

7. Conclusion

In this work, we have introduced a new 1D modeling approach to simulate blood flow in the cardiovascular system. Deriving the Lax–Friedrichs scheme from a model relaxation allows for a simple way to couple vessels in a network without relying on the eigenstructure of the regarding flow models. We have provided a second order scheme extension and showcased an adaptation of the approach to extended pressure models accounting for viscoelasticity of the vessel wall. Our numerical tests have confirmed consistency, efficiency and grid convergence of the proposed technique. The method, in particular, facilitates the extension of the one-dimensional modeling of arterial networks to biomedical applications; such computational hemodynamics applications will be subject of future work.

Notes

1. Our notion of conservative systems here neglects the viscous source term S_v.
2. The total pressure we consider here generalizes the form in [10], where $\alpha = 1$ is assumed.
3. The EOC is defined by $\text{EOC} = \log_2(e_1/e_2)$, where e_1 and e_2 are the errors in two consecutive lines of the table.

Disclosure statement

The authors declare there is no conflict of interest.

Funding

The authors thank the Deutsche Forschungsgemeinschaft (DFG, German Research Foundation) for the financial support under 320021702/GRK2326 (Graduate College Energy, Entropy, and Dissipative Dynamics), through SPP 2410 (Hyperbolic Balance Laws in Fluid Mechanics: Complexity, Scales, Randomness) within the Projects 526006304 and 525842915, through SPP 2311 (Robust Coupling of Continuum-Biomechanical In Silico Models to Establish Active Biological System Models for Later Use in Clinical Applications – Co-Design of Modelling, Numerics and Usability) within the Project 548864771 and though Project 461365406 (New traffic models considering complex geometries and data). Support by the ERS Open Seed Fund of RWTH Aachen University through project OPSF781 is also acknowledged.

References

Balossino R, Gervaso F, Migliavacca F, Dubini G. 2008. Effects of different stent designs on local hemodynamics in stented arteries. J Biomech. 41(5):1053–1061. doi:10.1016/j.jbiomech.2007.12.005.

Benemerito I, Mustafa A, Wang N, Narata AP, Narracott A, Marzo A. 2023. A multiscale computational framework to evaluate flow alterations during mechanical thrombectomy for treatment of ischaemic stroke. Front Cardiovasc Med. 10:1117449. doi:10.3389/fcvm.2023.1117449.

Bezanson J, Edelman A, Karpinski S, Shah VB. 2017. Julia: a fresh approach to numerical computing. SIAM Rev. 59(1):65–98. doi:10.1137/141000671.

Boileau E, Nithiarasu P, Blanco PJ, Müller LO, Fossan FE, Hellevik LR, Donders WP, Huberts W, Willemet M, Alastruey J. 2015. A benchmark study of numerical schemes for one-dimensional arterial blood flow modelling. Numer Methods Biomed Eng. 31(10):e02732. doi:10.1002/cnm.2732.

Chen G-Q, Levermore CD, Liu T-P. 1994. Hyperbolic conservation laws with stiff relaxation terms and entropy. Commun Pure Appl Math. 47(6):787–830. doi:10.1002/cpa.3160470602.

Crosetto P, Reymond P, Deparis S, Kontaxakis D, Stergiopulos N, Quarteroni A. 2011. Fluid–structure interaction simulation of aortic blood flow. Comput Fluids. 43(1):46–57. doi:10.1016/j.compfluid.2010.11.032.

Donea J, Giuliani S, Laval H, Quartapelle L. 1984. Time-accurate solution of advection-diffusion problems by finite elements. Comput Methods Appl Mech Eng. 45(1–3):123–145. doi:10.1016/0045-7825(84)90153-1.

Dubois F, Le Floch P. 1988. Boundary conditions for nonlinear hyperbolic systems of conservation laws. J Differ Equ. 71(1):93–122. doi:10.1016/0022-0396(88)90040-X.

Fleeter CM, Geraci G, Schiavazzi DE, Kahn AM, Marsden AL. 2020. Multilevel and multifidelity uncertainty quantification for cardiovascular hemodynamics. Comput Methods Appl Mech Eng. 365:113030–113037. doi:10.1016/j.cma.2020.113030.

Formaggia L, Lamponi D, Quarteroni A. 2003. One-dimensional models for blood flow in arteries. J Eng Math. 47(3/4):251–276. doi:10.1023/B:ENGI.0000007980.01347.29.

Formaggia L, Lamponi D, Tuveri M, Veneziani A. 2006. Numerical modeling of 1D arterial networks coupled with a lumped parameters description of the heart. Comput Methods Biomech Biomed Eng. 9(5):273–288. doi:10.1080/10255840600857767.

Formaggia L, Nobile F, Quarteroni A, Veneziani A. 1999. Multiscale modelling of the circulatory system: a preliminary analysis. Comput Visual Sci. 2(2–3):75–83. doi:10.1007/s007910050030.

Forti RM, Favilla CG, Cochran JM, Baker WB, Detre JA, Kasner SE, Mullen MT, Messé SR, Kofke WA, Balu R, et al. 2019. Transcranial optical monitoring of cerebral hemodynamics in acute stroke patients during mechanical thrombectomy. J Stroke Cerebrovasc Dis. 28(6):1483–1494. doi:10.1016/j.jstrokecerebrovasdis.2019.03.019.

Friedrichs KO, Lax PD. 1971. Systems of conservation equations with a convex extension. Proc Natl Acad Sci USA. 68(8):1686–1688. doi:10.1073/pnas.68.8.1686.

Fung YC, Cowin SC. 1994. Biomechanics: mechanical properties of living tissues, 2nd ed. J Appl Mech. 61(4):1007–1007. doi:10.1115/1.2901550.

Herty M, Kolbe N, Müller S. 2022. Central schemes for networked scalar conservation laws. NHM. 18(1):310–340. doi:10.3934/nhm.2023012.

Herty M, Kolbe N, Müller S. 2023. A central scheme for two coupled hyperbolic systems. Commun Appl Math Comput. 6:2093–2118. doi:10.1007/s42967-023-00306-5.

Herty M, Kolbe N, Neidlin M. 2024. A one-dimensional model for aspiration therapy in blood vessels. arXiv:2403.05494. doi:10.48550/arXiv.2403.05494.

Hu J, Jin S, Li Q. 2017. Asymptotic-preserving schemes for multiscale hyperbolic and kinetic equations. In: Rémi Abgrall, Chi-Wang Shu, editors. Handbook of numerical analysis. Vol. 18; Amsterdam: Elsevier; p. 103–129. doi:10.1016/bs.hna.2016.09.001.

Hughes TJ, Lubliner J. 1973. On the one-dimensional theory of blood flow in the larger vessels. Math Biosci. 18(1–2):161–170. doi:10.1016/0025-5564(73)90027-8.

Hussain A, Dar MNR, Arif A. 2025. A computational investigation using the nonnewtonian sisko model and finite element analysis to determine blood flow characteristics in trapezoidal stenosed arteries. Int J Mod Phys B. 39(15):2550126. doi:10.1142/S0217979225501267.

Jin S, Xin Z. 1995. The relaxation schemes for systems of conservation laws in arbitrary space dimensions. Commun Pure Appl Math. 48(3):235–276. doi:10.1002/cpa.3160480303.

Jin S. 2012. Asymptotic preserving (AP) schemes for multiscale kinetic and hyperbolic equations: a review. Riv Math Univ Parma (N.S.). 3(2):177–216.

Kolbe N, Herty M, Müller S. 2024. Numerical schemes for coupled systems of nonconservative hyperbolic equations. SIAM J Numer Anal. 62(5):2143–2171. doi:10.1137/23M1615176.

Kolbe N. 2022. Implementation of central schemes for networks of scalar conservation laws. *GitHub repository*. https://github.com/nklb/CentralNetworkScheme.

Kurganov A, Tadmor E. 2000. New high-resolution central schemes for nonlinear conservation laws and convection-diffusion equations. J Comput Phys. 160(1):241–282. doi:10.1006/jcph.2000.6459.

Liu T-P. 1987. Hyperbolic conservation laws with relaxation. Commun Math Phys. 108(1):153–175. doi:10.1007/BF01210707.

Lucca A, Busto S, Müller LO, Toro EF, Dumbser M. 2023. A semi-implicit finite volume scheme for blood flow in elastic and viscoelastic vessels. J Comput Phys. 495:112530. Paper No42, doi:10.1016/j.jcp.2023.112530.

Müller LO, Blanco PJ. 2015. A high order approximation of hyperbolic conservation laws in networks: application to one-dimensional blood flow. Comput Phys. 300:423–437. doi:10.1016/j.jcp.2015.07.056.

Müller LO, Toro EF. 2013. Well-balanced high-order solver for blood flow in networks of vessels with variable properties. Numer Methods Biomed Eng. 29(12):1388–1411. doi:10.1002/cnm.2580.

Mynard JP, Nithiarasu P. 2008. A 1D arterial blood flow model incorporating ventricular pressure, aortic valve and regional coronary flow using the locally conservative Galerkin (LCG) method. Commun Numer Meth Eng. 24(5):367–417. doi:10.1002/cnm.1117.

Neidlin M, Sonntag SJ, Schmitz-Rode T, Steinseifer U, Kaufmann TA. 2016. Investigation of hemodynamics during cardiopulmonary bypass: a multiscale multiphysics fluid–structure-interaction study. Med Eng Phys. 38(4):380–390. doi:10.1016/j.medengphy.2016.01.003.

Nobile F, Vergara C. 2008. An effective fluid-structure interaction formulation for vascular dynamics by generalized Robin conditions. SIAM J Sci Comput. 30(2):731–763. doi:10.1137/060678439.

Peiró J, Veneziani A. 2009. Reduced models of the cardiovascular system. In Cardiovascular mathematics, volume 1 of *MS&A. Model. Simul. Appl.*, pages p. 347–394. Springer Italia, Milan, doi:10.1007/978-88-470-1152-6_10.

Pradhan AM, Mut F, Cebral JR. 2024. A one-dimensional computational model for blood flow in an elastic blood vessel with a rigid catheter. Numer Methods Biomed Eng. 40(7):e3834. doi:10.1002/cnm.3834.

Quarteroni A, Formaggia L. 2004. Mathematical modelling and numerical simulation of the cardiovascular system. In: Ciarlet PG, editor. Handbook of numerical analysis. Vol. XII. North Holland, Amsterdam: Elsevier; p. 3–127. doi:10.1016/S1570-8659(03)12001-7.

Saini V, Guada L, Yavagal DR. 2021. Global epidemiology of stroke and access to acute ischemic stroke interventions. Neurology. 97(20 Suppl 2):S6–S16. doi:10.1212/wnl.0000000000012781.

Segers P, Stergiopulos N, Westerhof N, Wouters P, Kolh P, Verdonck P. 2003. Systemic and pulmonary hemodynamics assessed with a lumped-parameter heart-

arterial interaction model. J Eng Math. 47(3/4):185–199. 10.1023/B:ENGI.0000007975.27377.9c.
Smith NP, Pullan AJ, Hunter PJ. 2002. An anatomically based model of transient coronary blood flow in the heart. SIAM J Appl Math. 62(3):990–1018. doi:10.1137/S0036139999355199.
Steele B, Wan J, Ku J, Hughes T, Taylor C. 2003. In vivo validation of a one-dimensional finite-element method for predicting blood flow in cardiovascular bypass grafts. IEEE Trans Biomed Eng. 50(6):649–656. doi:10.1109/TBME.2003.812201.
Thompson KW. 1987. Time dependent boundary conditions for hyperbolic systems. J Comput Phys. 68(1):1–24. doi:10.1016/0021-9991(87)90041-6.
Toro EF, Siviglia A. 2013. Flow in collapsible tubes with discontinuous mechanical properties: mathematical model and exact solutions. Commun Comput Phys. 13(2):361–385. doi:10.4208/cicp.210611.240212a.
van Leer B. 1979. Towards the ultimate conservative difference scheme. V. A second-order sequel to Godunov's method. J Comput Phys. 32(1):101–136. doi:10.1016/0021-9991(79)90145-1.
Wang X, Fullana J-M, Lagrée P-Y. 2015. Verification and comparison of four numerical schemes for a 1d viscoelastic blood flow model. Comput Methods Biomech Biomed Eng. 18(15):1704–1725. doi:10.1080/10255842.2014.948428.
White F. 1991. Viscous fluid flow. McGraw-Hill series in mechanical engineering. New York: McGraw-Hill.
Wilkins E, Wilson L, Wickramasinghe K, Bhatnagar P, Leal J, Luengo-Fernandez R, Burns R, Rayner M, Townsend N. 2017. European Cardiovascular Disease Statistics 2017. Brussels: EHN.

Appendix A. A computation of the coupling data in the one-to-one coupling problem

In this appendix a procedure to solve the nonlinear system in Section 5.1 is described. For the sake of simplicity we assume $\alpha = 1$. In the first step we eliminate the variables $\mathbf{V}_R$ and $\mathbf{V}_L$ in the system. To this end we exploit (22) in (29) and (30) and obtain

$$\left[\mathbf{F}^I(\mathbf{U}_N^I)\right]_1 + \lambda\left(A_N^I - A_R\right) = \left[\mathbf{F}^{II}(\mathbf{U}_1^{II})\right]_1 + \lambda\left(A_L - A_1^{II}\right), \tag{40}$$

$$\begin{aligned}\left[\mathbf{F}^I(\mathbf{U}_N^I)\right]_2 + \lambda\left(Q_N^I - Q_R\right) =& \frac{\alpha}{2}\frac{Q_R^2}{A_R} - \frac{\alpha}{2}\frac{A_R Q_L^2}{A_L^2} \\ &+ \frac{A_R}{A_L}\left(\left[\mathbf{F}^{II}(\mathbf{U}_1^{II})\right]_2 + \lambda(Q_L - Q_1^{II})\right) \\ &+ \frac{1}{\rho}\left(\frac{A_R}{A_L}P(A_L; A_0^{II}, \beta^{II}) - P(A_R; A_0^I, \beta^I)\right),\end{aligned} \tag{41}$$

where in the numerical data near the interface and the flux function the corresponding edge is indicated by I or II and $[\mathbf{v}]_i$ refers to the i-th component of a given vector $\mathbf{v}$.

It remains to solve the system given by (27, 28, 40) and (41) for the coupling data A_L, Q_L, A_R, Q_R; we note that all other variables are known parameters. To this end we first write Q_L as function $Q_L(Q_R) = Q_R$ of Q_R using (27), i.e. we replace Q_L by Q_R in the other equations. Next, (40) is used to rewrite A_L as

$$A_L(A_R) = \frac{1}{\lambda}\left(\left[\mathbf{F}^I(\mathbf{U}_N^I)\right]_1 - \left[\mathbf{F}^{II}(\mathbf{U}_1^{II})\right]_1\right) + A_N^I + A_1^I - A_R. \tag{42}$$

These two new expressions are inserted into (41), which results in a quadratic equation in Q_R with coefficients depending only on A_R that reads

$$\begin{aligned}&\left(\frac{1}{2}\frac{1}{A_R} - \frac{1}{2}\frac{A_R}{A_L(A_R)^2}\right)Q_R^2 + \left(\lambda + \frac{A_R}{A_L(A_R)}\lambda\right)Q_R \\ &+ \frac{A_R}{A_L(A_R)}\left(\left[\mathbf{F}^{II}(\mathbf{U}_1^{II})\right]_2 - \lambda Q_1^{II}\right) \\ &+ \frac{1}{\rho}\left(\frac{A_R}{A_L}P(A_L; A_0^{II}, \beta^{II}) - P(A_R; A_0^I, \beta^I)\right) \\ &- \left[\mathbf{F}^I(\mathbf{U}_N^I)\right]_2 - \lambda Q_N^I = 0.\end{aligned} \tag{43}$$

If $A_L(A_R) = A_R$ the quadratic term in (43) vanishes and we have

$$\begin{aligned}Q_R^1(A_R) = &\frac{1}{2\lambda}\left(\left[\mathbf{F}^I(\mathbf{U}_N^I)\right]_2 + \lambda Q_N^I - \left[\mathbf{F}^{II}(\mathbf{U}_1^{II})\right]_2 + \lambda Q_1^{II}\right) \\ &- \frac{1}{2\rho\lambda}\left(P(A_L; A_0^{II}, \beta^{II}) - P(A_R; A_0^I, \beta^I)\right).\end{aligned}$$

Otherwise, we obtain the two solutions

$$\begin{aligned}Q_R^{1,2}(A_R) = &-\frac{\lambda A_R A_L(A_R)}{A_L(A_R) - A_R} \\ &\pm\left(\frac{\lambda^2 A_R^2 A_L(A_R)^2}{(A_L(A_R) - A_R)^2} + \frac{2A_R A_L(A_R)^2}{A_L(A_R)^2 - A_R^2}\right. \\ &\times\left(\left[\mathbf{F}^I(\mathbf{U}_N^I)\right]_2 + \lambda Q_N^I - \frac{A_R}{A_L(A_R)}\left(\left[\mathbf{F}^{II}(\mathbf{U}_1^{II})\right]_2 - \lambda Q_1^{II}\right)\right. \\ &\left.\left.- \frac{1}{\rho}\left(\frac{A_R}{A_L}P(A_L; A_0^{II}, \beta^{II}) - P(A_R; A_0^I, \beta^I)\right)\right)\right)^{1/2}.\end{aligned}$$

Substituting either $Q_R^1(A_R) = Q_L$ or $Q_R^2(A_R) = Q_L$ into (28) together with $A_L(A_R)$ gives rise to a nonlinear equation in A_R, which is solved numerically (e.g. using Newtons method). By re-substituting we then obtain the remaining coupling data. If multiple solutions to the system are obtained, we select the one that is closest to the trace data $\mathbf{U}_N^I$ and $\mathbf{U}_1^{II}$ in the sense of L^1-distance.